J Mater Sci (2021) 56:10640–10652

Metals & corrosion

Surface deformation of single crystalline copper on different nano-scratching paths

Jinxuan Zhu[1], Qinghua Zhou[1,*], Yanyan Huang[2], Bo Zhou[1], and Jiaxu Wang[1]

[1] School of Aeronautics and Astronautics, Sichuan University, Chengdu 610065, China
[2] School of Mechanical Engineering, Chengdu University, Chengdu 610106, China

Received: 22 September 2020
Accepted: 17 February 2021
Published online: 3 March 2021

ABSTRACT

Anisotropic deformation behavior of single crystalline material under scratching has a significant effect on machining precision in nano-mechanical machining. In the present work, a crystal plasticity finite element model simulating the scratching process is developed, and the established model is validated by comparison with experimental results. (001)-, (101)- and (111)-oriented coppers are selected to investigate the deformation behavior including scratching depth, surface topography and subsurface deformation affected by scratching path. Further, the deformation mechanisms of (001)-, (101)- and (111)-oriented coppers are analyzed to be caused by deformation of slip systems.

Introduction

More recently, nano/micro- structure machining has been attracted more and more attentions, due to the increasing need in the fields such as micro-electromechanical systems [1]. Atomic force microscopy (AFM) tip-based nano-mechanical machining has been widely adopted to fabricate nano-structures on different materials, such as metals [2], polymers [3] and semi-conductors [4], due to its relatively low cost and ease of operation. The machining process is the same as a scratching process that a tip scratches the specimen surface with a predefined normal load and scratching path. Different deformation behavior would lead to different scratching depths and topographies. Therefore, it is meaningful to conduct a thorough research on deformation behavior of target material under scratching, so as to improve machining precision.

Copper is one of the materials commonly adopted to fabricate nano/micro- structures, and it is usually composed of a lot of fine grains which exhibit anisotropic mechanical behavior at nano/micro- scale. Since nano-mechanical machining is implemented at grain-scale (single or several grains), the effect of anisotropic behavior of single crystalline copper cannot be ignored. Crystallographic orientation has a

Handling Editor: N. Ravishankar.

Address correspondence to E-mail: qh.zhou@foxmail.com

https://doi.org/10.1007/s10853-021-05948-5

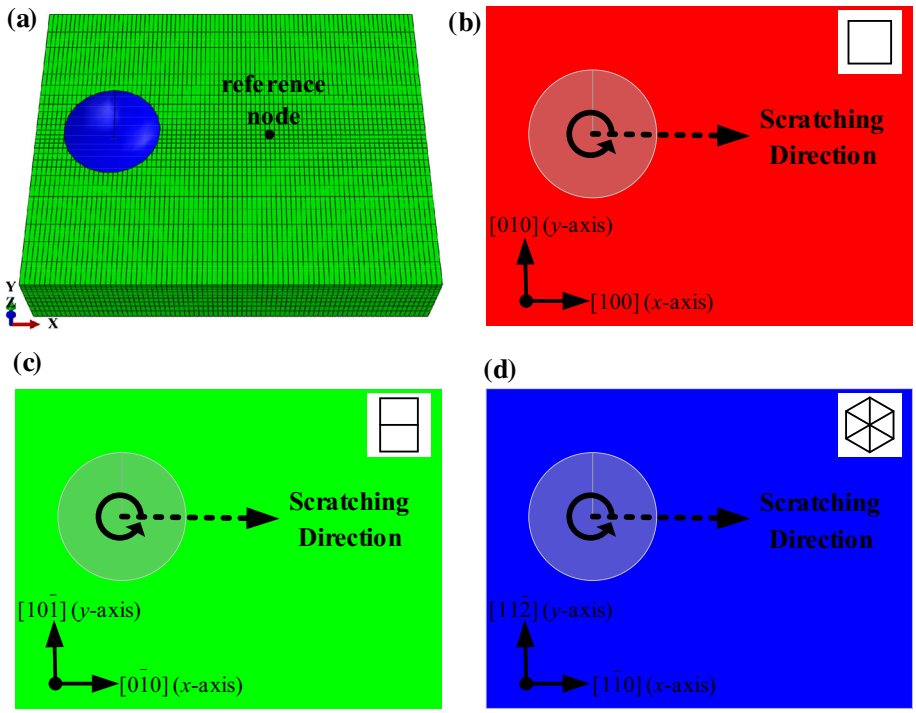

Figure 1 Configuration of nano-scratching simulation. **a** Nano-scratching model, schemes of scratching directions in the cases of **b** (001)-, **c** (101)- and **d** (111)-oriented coppers.

Table 1 Mechanical properties of single crystal copper

Parameters	C_{11} (MPa)	C_{12} (MPa)	C_{44} (MPa)	$\dot{\gamma}_0$ (s^{-1})	m (-)	n (-)	h_0 (MPa)	τ_c^{α} (MPa)	τ_s (MPa)
Values	168,400	121,400	75,400	1×10^{-9}	13	3	110	32	100

significant effect on anisotropic behavior which has been studied by many research works. Zambaldi et al. [5] investigated the plastic anisotropy behavior of γ-TiAl and predicted the indented surface pile-ups of γ-TiAl with different crystallographic orientations. Wang et al. [6] studied the evolution of crystallographic textures of (001)-, (011)- and (111)-oriented coppers under nano-indenting. Experimental test and simulation were employed by Liu et al. [7] to investigate the mechanical properties of single crystalline aluminum with different crystallographic orientations. However, crystallographic orientation is not the only factor that affects anisotropic behavior significantly. Single crystalline copper would also exhibit different mechanical behavior when a tip scratches along different directions, even if the crystallographic orientation of copper does not change. For example, the scratching force of (001)-oriented copper along the [110] direction is greater than that of the [100] direction [8].

Nano-scratching, a test technique that making a specimen plastically deformed along a given scratching direction [9], is an effective testing method which has been widely adopted to study scratching behavior of anisotropic materials [10–14]. Numerical simulation, commonly recognized as an important supplementary of experimental investigation, is an effective method to investigate deformation mechanism at nano/micro- scale. Crystal plasticity finite element method (CPFEM) is a method proposed to model micro-structure of crystalline material, which has been widely employed to simulate deformation processes, such as nano-indentation [15], uniaxial tension [16], compression [17] and torsion [18]. More recently, several publications introduced the CPFEM models to study the machining and scratching behavior of crystalline materials. Wang et al. [19] developed a CPFEM model simulating the cutting process of polycrystalline copper to investigate the effect of grain boundaries on the microscopic deformation behavior, comparing to the macroscopic machining results. Wang et al. [20] employed the CPFEM to investigate the pile-up behavior of (010)-, $(\bar{1}01)$- and $(\bar{1}11)$-oriented copper by simulating the

Berkovich nano-scratching process, but the scratching direction was not taken into consideration in their work. The simulating results in these works are in good agreements with the corresponding experimental results.

The present work aims to investigate the surface deformation of single crystalline copper on different scratching paths, and the CPFEM model simulating the nano-scratching process is developed. Further, the scratching depth, surface topography and subsurface deformation induced by a tip that scratches along different directions are studied in detail for the cases of (001)-, (101)- and (111)-oriented coppers.

Methods

Phenomenological constitutive model

The CPFEM constitutive model adopted in this work is a phenomenological model which considers dislocation slip as the only deformation mechanism and takes critical resolved shear stress (CRSS) as the state variable for each slip system. As the resolved shear stress on a slip plane reaches the CRSS, dislocation slip will be triggered. Phenomenological model is a kind of effective constitutive models that has been employed by many research works [21–25] to describe the deformation behavior of crystalline material. More details about it can be found in Ref. [26].

CPFEM model implementation

ABAQUS (Simulia 2017) and Düsseldorf Advanced Material Simulation Kit (DAMASK) [27] are employed to implement CPFEM simulation in the present work. The utilized CPFEM model simulating nano-scratching process has a total of 19,422 elements and 22,680 nodes, as shown in Fig. 1a. The dimensions of single crystalline copper specimen are $25 \times 20 \times 5\ \mu m^3$ (X × Y × Z), and the mechanical parameters of copper are listed in Table 1 [28]. To ensure both simulation accuracy and computational efficiency, the copper specimen is meshed by using a transition mesh technique, and the meshes around contact region are much finer than those of the other regions. The diamond spherical tip with a radius of 5 μm is simplified as a rigid body due to its far greater hardness than that of single crystalline copper to improve computational efficiency.

In this work, the direction paralleled to the x-axis is set as initial scratching direction which is designated as Direction 0° here. The [100], $[0\bar{1}0]$ and $[1\bar{1}0]$ directions are therefore the corresponding initial scratching directions for (001)-, (101)- and (111)-oriented coppers, respectively, shown in Fig. 1b–d. The nano-scratching simulations for (001)-, (101)- and (111)-oriented coppers are all performed along 25 different scratching directions which increase counterclockwise from 0° to 360° with an interval of 15°. The selected typical nano-scratching is composed of loading stage, scratching stage and unloading stage. In the first stage, the tip is penetrated into the specimen by applying a normal force of 6 mN with a constant rate of 3 mN/s. Then the tip scratches 15 μm with a specific speed of 1 μm/s along one scratching direction. Finally, unloading the tip in 2 s at a constant rate in the last stage. The bottom surface of specimen is fixed, and the tip can only scratch along the x and z axes (shown in Fig. 1a). The friction coefficient between specimen surface and indenter is not taken into consideration in this work.

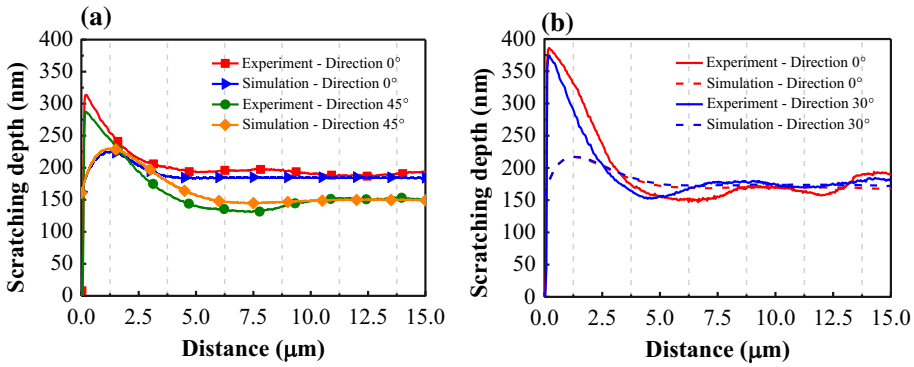

Figure 2 Scratching depth-distance curves of **a** (001)- and **b** (111)-oriented coppers produced by experimental tests and CPFEM simulations.

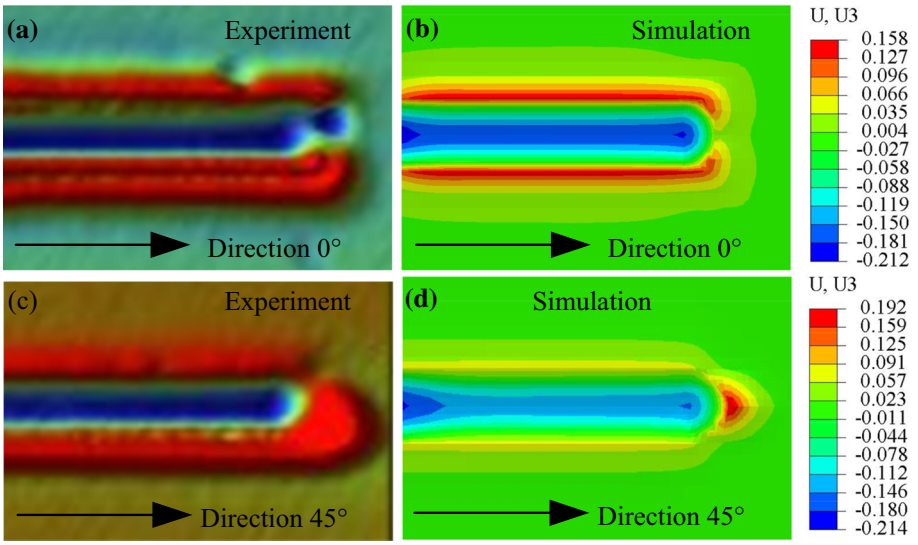

Figure 3 Topographies of (001)-oriented copper induced by a tip which scratches along different nano-scratching directions. **a** Direction 0° (experiment), **b** Direction 0° (simulation), **c** Direction 45° (experiment), **d** Direction 45° (simulation).

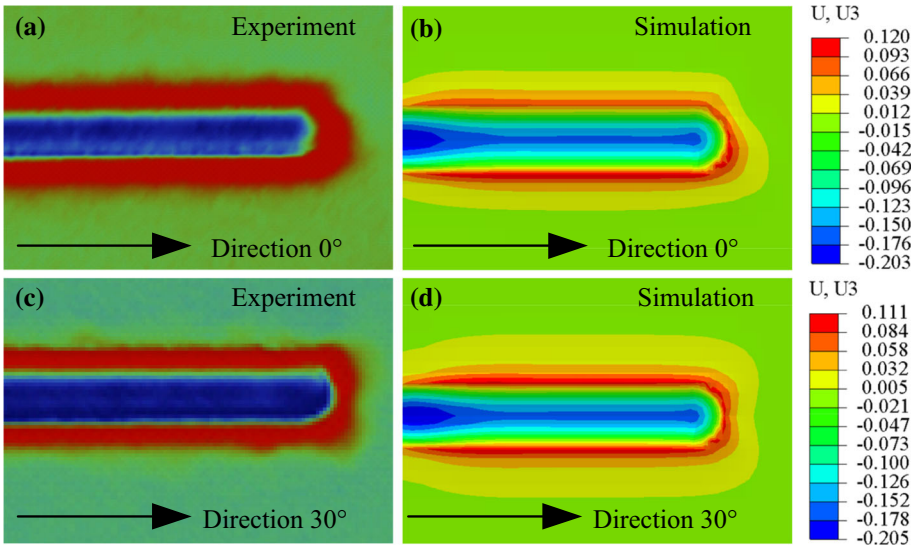

Figure 4 Topographies of (111)-oriented copper induced by a tip which scratches along different nano-scratching directions. **a** Direction 0° (experiment), **b** Direction 0° (simulation), **c** Direction 30° (experiment), **d** Direction 30° (simulation).

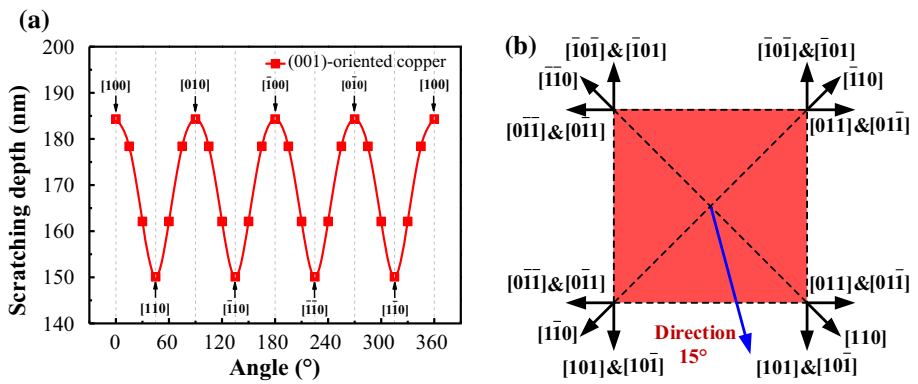

Figure 5 **a** Scratching depths when a tip scratches along different scratching directions. **b** Schematic illustration of slip systems of (001)-oriented copper.

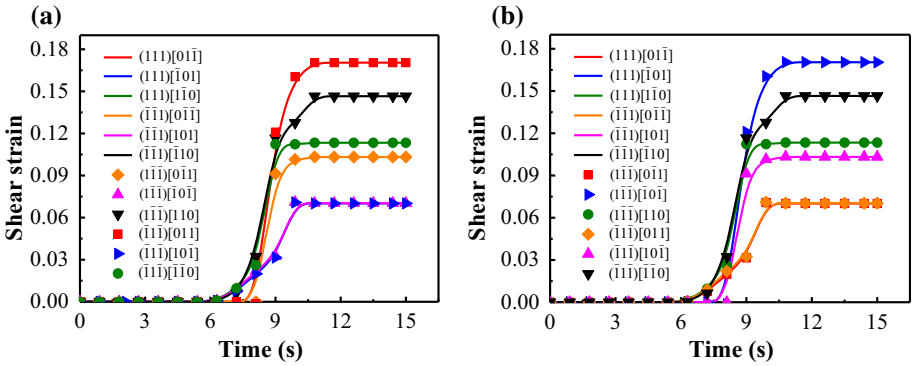

Figure 6 Evolution of accumulated shear strain of slip systems of when a tip scratches along **a** Direction 0°, and **b** Direction 90°.

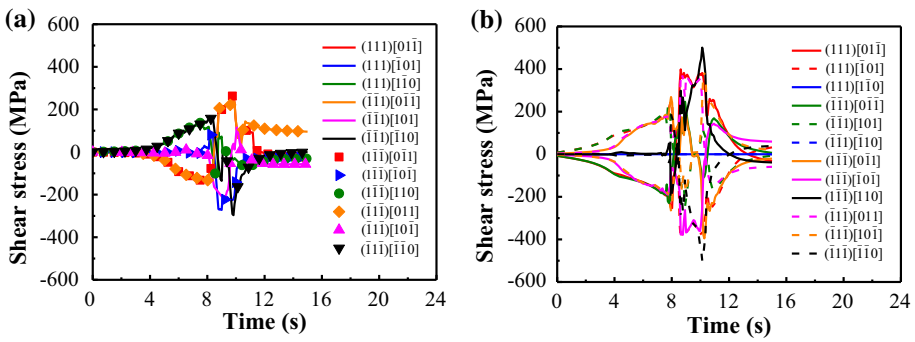

Figure 7 Evolution of resolved shear stress of the reference node when a tip scratches along **a** Direction 90°, and **b** Direction 45°.

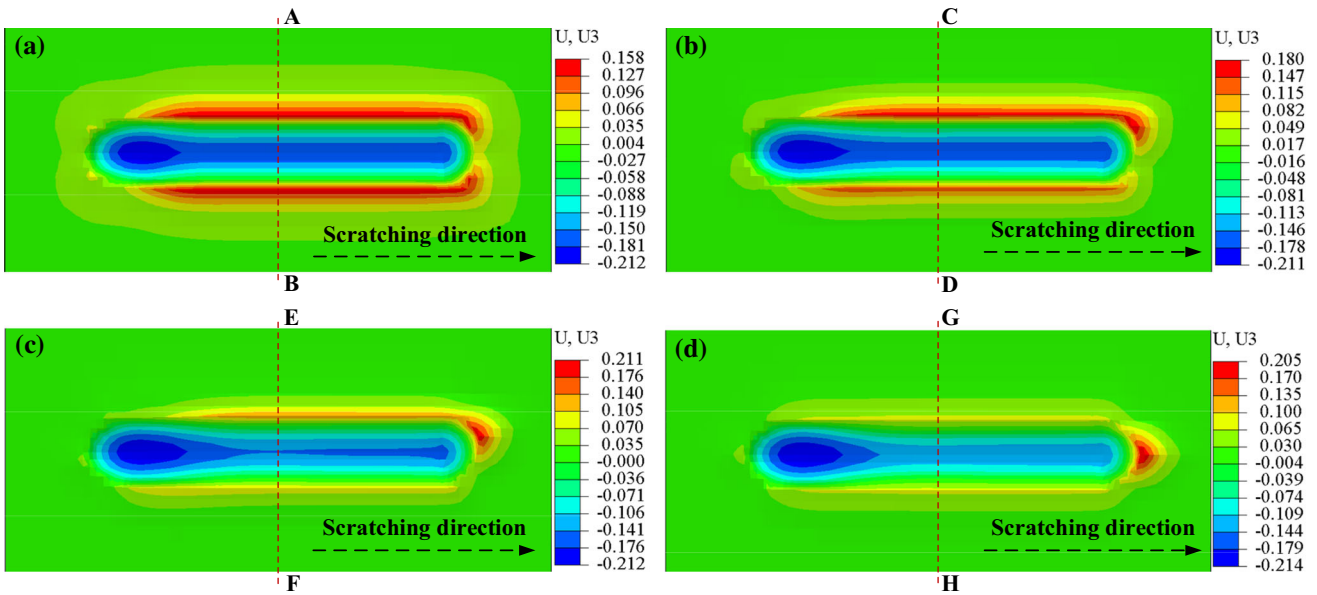

Figure 8 Simulated topography pile-ups after scratching along different directions, **a** Direction 0°, **b** Direction 15°, **c** Direction 30°, **d** Direction 45°.

Experimental configuration of nano-scratching

Mechanically and chemically polished high-purity (001)- and (111)-oriented coppers with surface roughness of less than 10 nm (supplied by the Hefei Kejing Materials Technology Co., Ltd) are adopted to implement nano-scratching tests. Both the specimens have cuboid sizes of 10 mm in length × 10 mm in width × 1 mm in height. The employed spherical indenter with a tip radius of 5 μm is made of diamond. Nano-scratching tests are all implemented by

a nano-indentation instrument (Micro Materials Ltd, Wrexham, UK) under a room temperature (25 °C). Except for the loading stage, the experimental parameters are consistent with those of simulation. In experimental test, the specimen is first accelerated to 1 μm/s, and then a normal force of 6 mN is applied promptly on the indenter to make it penetrate into the specimen while keeping the specimen velocity unchanged, due to the restricted loading mode of the employed instrument. The scratched surface topographies are measured by a Bruker Contour GT-K Optical Profile.

Verification of simulation models

Figure 2a, b show the scratching depth-distance curves of (001)- and (111)-oriented coppers obtained from both experiments and simulations. In general, the scratching depths of simulations are in good agreement with those of experimental tests. The depth differences between experimental tests and simulations at the initial stage are attributed to the difference of loading mode, as stated in Sect. 2.3. The residual topographies formed on (001)- and (111)-oriented coppers are presented in Figs. 3 and 4. The simulation topographies are also in well agreement with the experimental results. The experimental topography induced by nano-scratching in the case of Direction 45° in Fig. 3 shows a lower level of symmetry than that of the simulation one, which may be attributed to the positioning accuracy in experiment. The simulation model employed by the present work is generally accurate enough to study the deformation behavior of single crystalline copper.

Results and discussions

Deformation behavior of (001)-oriented copper

Figure 5a illustrates the scratching depth variations for (001)-oriented copper with respect to scratching direction produced by simulations. Scratching depth changes periodically with a period of 90°. It decreases gradually with the increase of direction angle in the first half period, then increases in the next half period. Besides, the maximum and minimum depths are observed on the < 100 > and < 110 > directions, respectively, and the maximum value is about 22.8% larger than the minimum one, indicating that scratching direction has a significant effect on the scratched depth.

The periodic variation of scratching depth can be attributed to the projected symmetric slip systems of (001)-oriented copper, as shown in Fig. 5b. There are four symmetrical axes for the slip systems, and the corresponding scratching directions paralleled to the

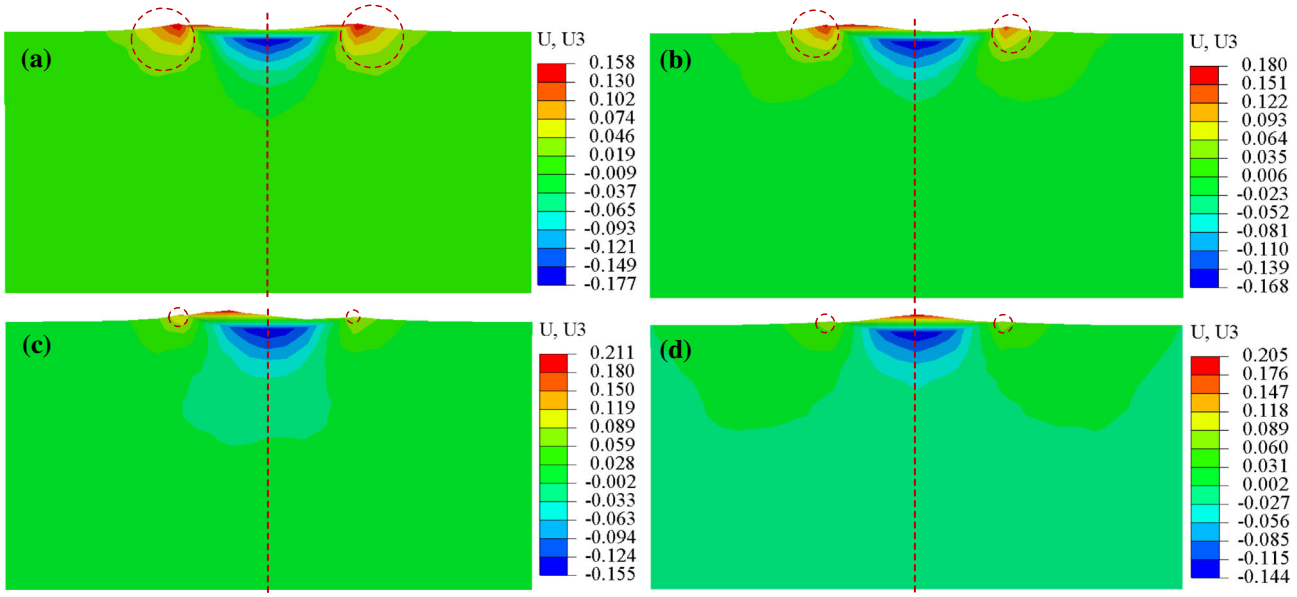

Figure 9 Subsurface deformation induced by a tip that scratches along **a** Direction 0°, **b** Direction 15°, **c** Direction 30° and **d** Direction 45°.

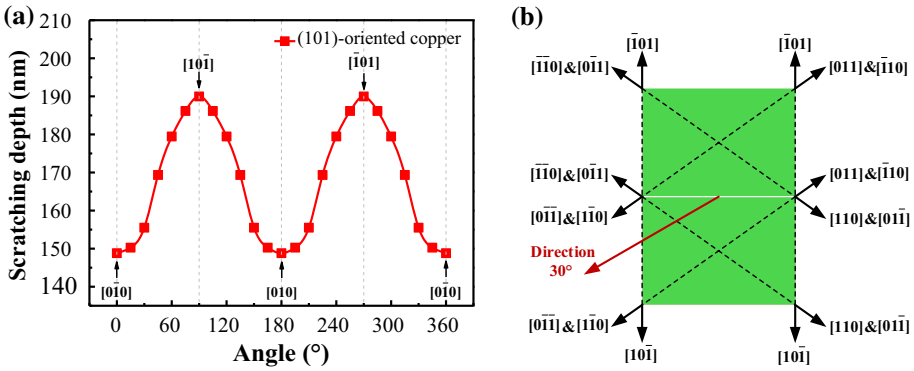

Figure 10 **a** Scratching depths when a tip scratches along different scratching directions. **b** Schematic illustration of slip systems of (101)-oriented copper.

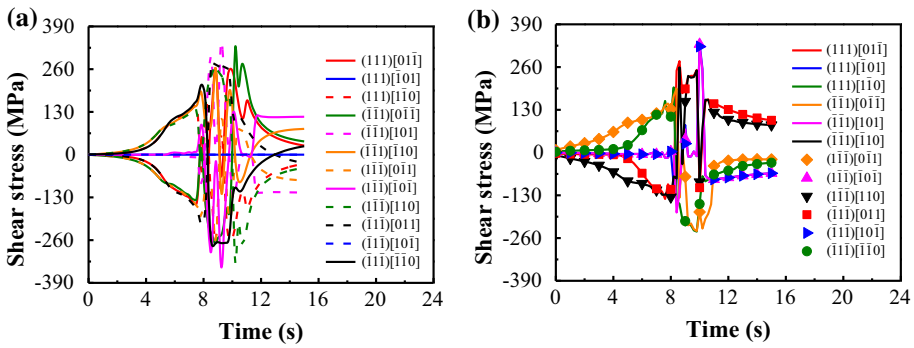

Figure 11 Evolution of resolved shear stress of the reference node when a tip scratches along **a** Direction 0°, and **b** Direction 90°.

four symmetrical axes are Directions 0° (or 180°), 45° (or 225°), 90° (or 270°) and 135° (or 315°), respectively. As the tip scratches along two directions which are symmetrical to each other, the deformations of slip systems in the two cases are also identical. For example, the shear strains of slip systems shown in Fig. 6 reveal that the maximum strain values in the cases of Directions 0° and 90° are equal to each other, and their corresponding slip systems (the $(111)[01\bar{1}]$ and $(1\bar{1}\bar{1})[\bar{1}0\bar{1}]$ slip systems) are symmetrical to each other along the symmetrical axis. Therefore, the two

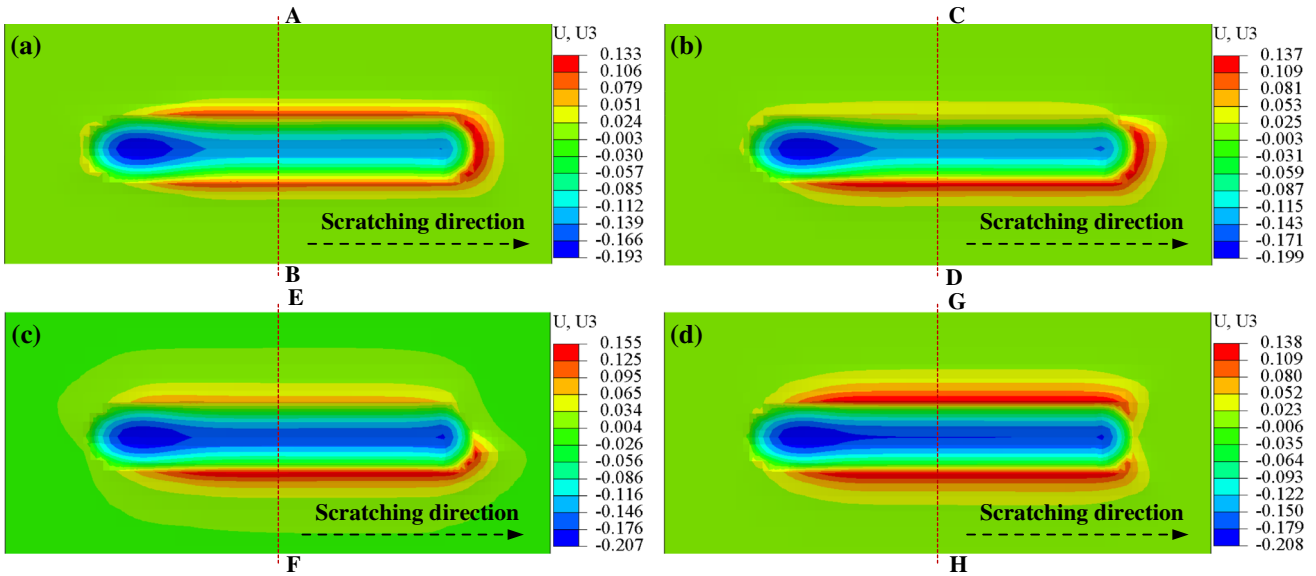

Figure 12 Simulated topology pile-ups after scratching along different directions, **a** Direction 0°, **b** Direction 30°, **c** Direction 60°, **d** Direction 90°.

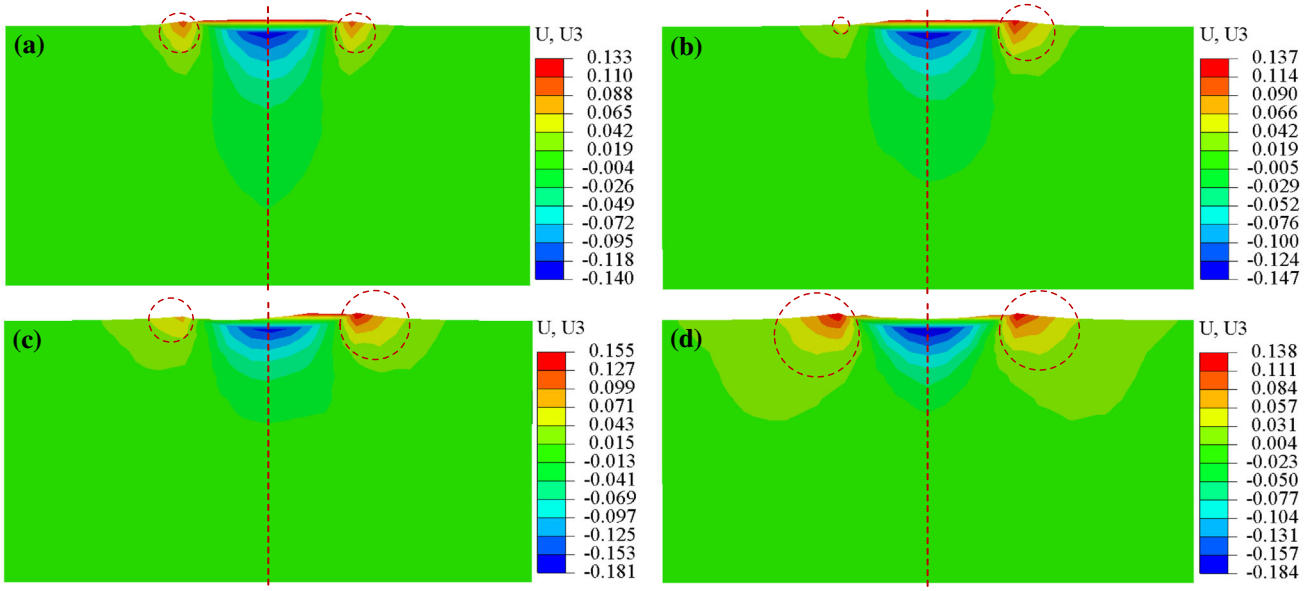

Figure 13 Subsurface deformation induced by a tip which scratches along **a** Direction 0°, **b** Direction 30°, **c** Direction 60° and **d** Direction 90°.

Figure 14 **a** Scratching depths when a tip scratches along different scratching directions. **b** Schematic of slip systems of (111)-oriented copper.

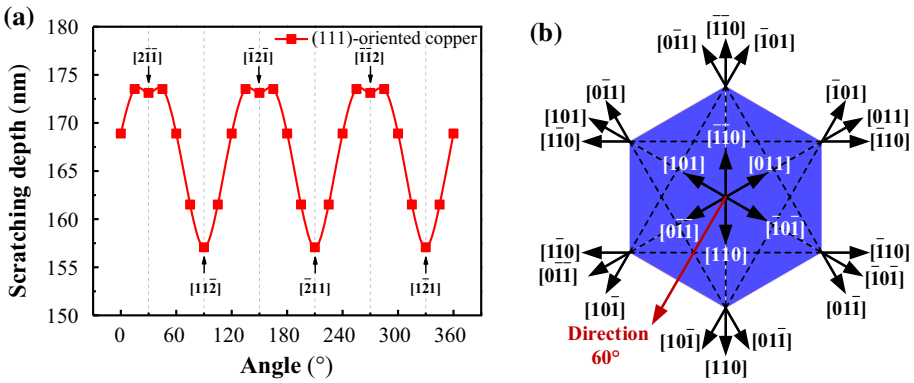

Figure 15 Evolution resolved shear stress of the reference node when a tip scratches along **a** Direction 30° and **b** Direction 90°.

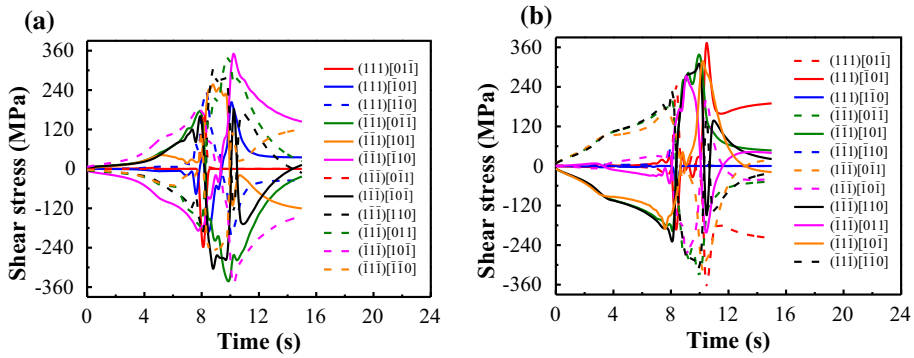

scratching depths are equal to each other when the two directions are symmetrical.

Figure 7a, b shows the resolved shear stresses of 12 slip systems of reference node (shown in Fig. 1a) when a tip scratches along Directions 90° and 45°, respectively. The resolved stresses in the case of Direction 45° are much greater than those of Direction 90°, which means that the slip systems tend to

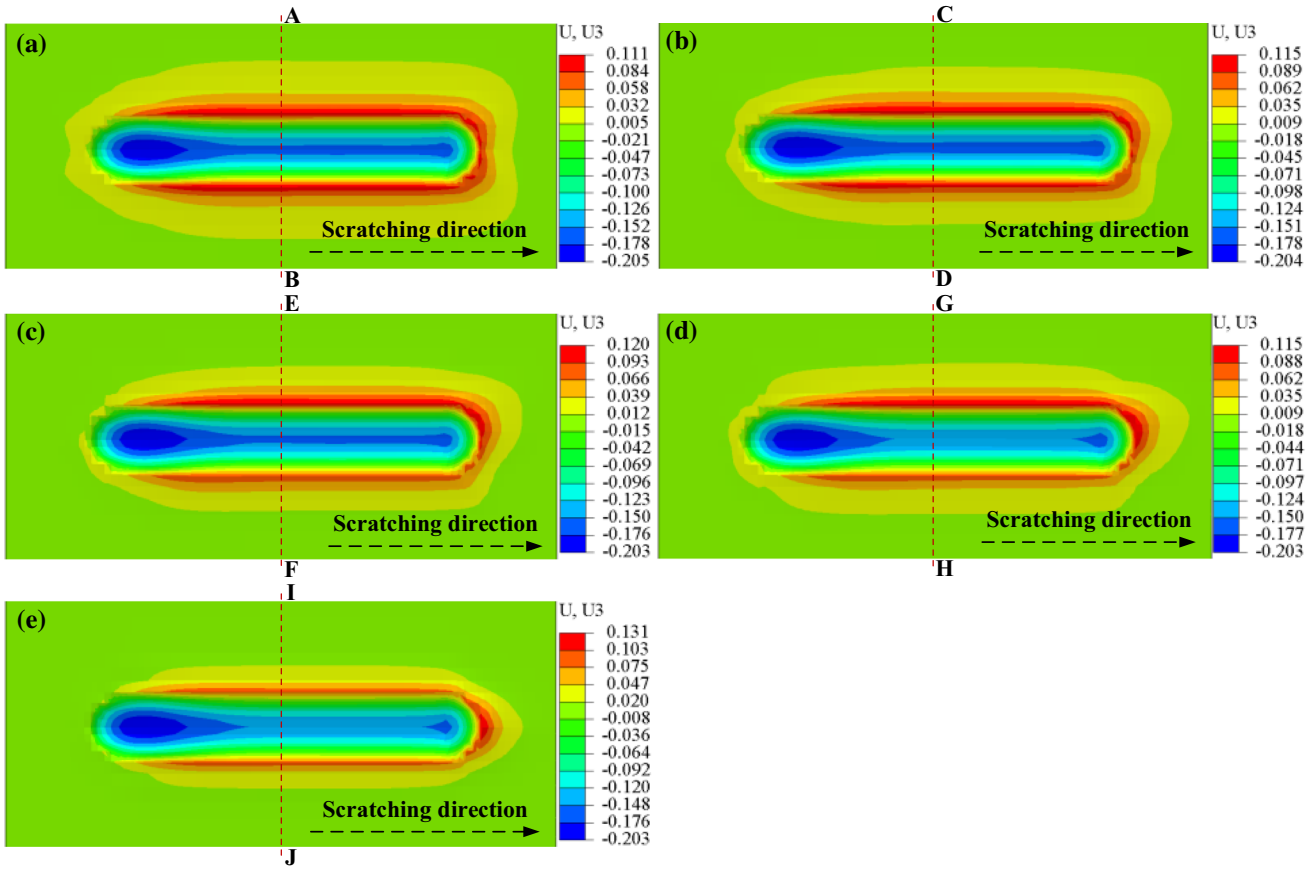

Figure 16 Simulated topography pile-ups of (111)-oriented copper after scratching along different directions, **a** Direction 30°, **b** Direction 45°, **c** Direction 60°, **d** Direction 75° and **e** Direction 90°.

form greater reaction forces. Since the resultant force along the normal direction (the indent direction) produced by deformation of slip systems is a constant (6mN), the (001)-oriented copper tends to produce less deformation as the tip scratches along Direction 45°. Therefore, the scratching depth in the case of Direction 45° is smaller than that of Direction 90°.

Figure 8a–d illustrates the pile-ups induced by a tip that scratches along Directions 0°, 15°, 30° and 45°, respectively. Significant differences can be observed on the pile-ups of the right ends (where the scratching ends). For the cases of Directions 0° and 45°, the induced pile-ups are symmetric with themselves along the scratching directions. While the pile-ups of the other two cases are asymmetric, and the pile-up heights on the left-side of scratching direction are greater than those of the right-side. Since the slip systems laid symmetrically with respect to Directions 0° and 45°, the slip systems in the two cases tend to deform symmetrically along the scratching direction. Further, when a tip scratches along Direction 15° or 30°, the slip systems on the left-side of scratching direction (shown in Fig. 5b) are more prone to be triggered than those of the right-side, due to the relatively higher density of slip systems and smaller angles between scratching direction and slip systems. Thus, the pile-up heights on the left-side are larger than those of the right-side.

Figure 9a–d shows the sections vertically cutting along the dash lines AB, CD, EF and GH in Fig. 8a–d, respectively. Apparently, positive displacements along the scratching direction in subsurface are observed for the regions on the left- and right-sides of the tip, indicating that materials at specific local regions around the tip tend to flow upwards. For the cases from Direction 0° to Direction 45°, the main uplifted region decreases gradually. It is clear that scratching direction is important to plastic flow in the subsurface of (001)-oriented copper.

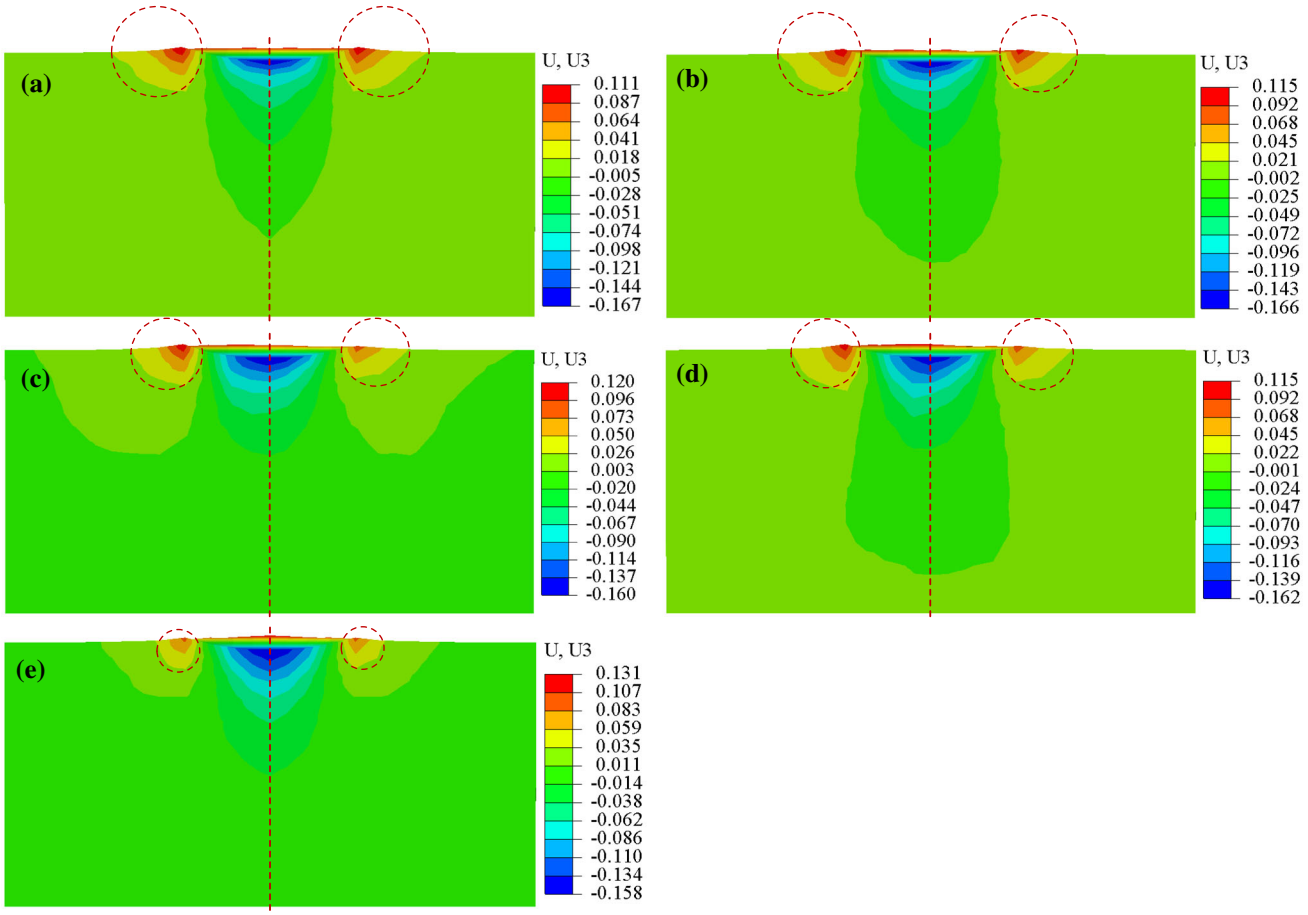

Figure 17 Subsurface deformation induced by a tip which scratches along **a** Direction 30°, **b** Direction 45°, **c** Direction 60°, **d** Direction 75° and **e** Direction 90°.

Deformation behavior of (101)-oriented copper

The simulated scratching depths when a tip scratches along different directions on (101)-oriented copper are shown in Fig. 10a. Similar to the case of (001)-oriented copper, the scratching depth also changes periodically with the variation of scratching direction. However, the period in the present case is 180° instead of 90°. Further, the maximum and minimum depths are observed in the cases of < 110 > and < 100 > directions, respectively, which are the opposite of the case of (001)-oriented copper, indicating that a (101)-oriented copper tends to produce larger plastic deformation as a tip scratches along the < 110 > directions. The difference between the maximum and minimum depths is about 27.7%, which is a bit larger than that of (001)-oriented copper case (22.8%).

The slip systems of (101)-oriented copper with respect to the scratched surface are demonstrated in Fig. 10b. There are two symmetrical axes of slip systems for (101)-oriented copper, and they are parallel to Directions 0° (or 180°) and 90° (or 270°), respectively. The scratching depths when a tip scratches along the directions on the right-side of the symmetrical axes (such as Direction 45°) are equal to those of directions (such as Direction 135°) on the left-side. Therefore, the two symmetrical axes lead to the periodical variation of scratching depth, and the period is 180°.

Figure 11a, b shows the resolved shear stresses when a tip scratches along Directions 0° and 90°, respectively. Compared with the case of Direction 90°, the shear stresses of the other case are generally larger so that a (101)-oriented copper deforms less in the normal direction when a tip scratches along Direction 0°.

The surface topographies of (101)-oriented copper fabricated by a tip which scratches along Directions 0°, 30°, 60° and 90° are shown in Fig. 12a–d, respectively. Similar to the case of (001)-oriented copper, there are two types of topographies, i.e., topographies symmetrical and asymmetric along the scratching direction. Since Directions 0° and 90° are parallel to the symmetrical axes of slip systems, the pile-ups are symmetrical along the scratching directions in the two cases. Moreover, the greater pile-up heights observed on the right-side in the cases of Directions 30° and 60° can be attributed to the denser located slip systems on the right-side (shown in Fig. 10b).

The subsurface deformation of (101)-oriented copper induced by scratching is shown in Fig. 13. Similar to the case of (001)-oriented copper, there are also regions with positive displacement on the left- and right- sides beneath the surface. Further, with the increase of scratching direction angle, the effected regions become larger instead of smaller, compared to the cases of (001)-oriented copper. However, a larger scratched depth results in a larger uplifted region for both the cases of (001)- and (101)-oriented coppers.

Deformation behavior of (111)-oriented copper

The scratching depth for the case of (111)-oriented copper shown in Fig. 14a reveals that the depth changes periodically with a period of 120°, and both the maximum and minimum depths arise when the scratching direction is parallel or near to the $< 112 >$ directions. The maximum depth is about 10.5% greater than the minimum value, which is smaller than those of (001)-oriented copper (22.8%) and (101)-oriented copper (27.7%) cases. Figure 14b illustrates the slip systems of (111)-oriented copper beneath the scratching surface. By computing the angles between the normal direction (the [111] direction) and slip directions, it is easy to observe that all the [101], [011] and [110] slip directions have an angle of 35.26° with respect to the normal direction. While the angle is 144.74° when the slip directions are $[\bar{1}10]$, $[0\bar{1}1]$ and $[\bar{1}0\bar{1}]$. Therefore, the slip systems are asymmetrical along Directions 0° (or 180°), 60° (or 300°) and 120° (or 240°), but symmetrical along Directions 30° (or 210°), 90° (or 180°) and 150° (or 330°), instead. Therefore, according to the discussion in Sect. 3.1, the period becomes 120° instead of 60° in the present case.

The resolved stress variations of the reference node in the cases of Directions 30° and 90° are plotted in Fig. 15a, b. There has little difference between the shear stresses of the two cases. The stress values of the latter case are a little larger than those of the former case. Therefore, the corresponding scratching depth is greater when a tip scratches along Direction 30°, but the difference between the maximum and minimum depths is relatively small compared to those of the (001)- and (101)-oriented coppers.

The pile-ups of (111)-oriented copper are shown in Fig. 16a–e. Similar to (001)- and (101)-oriented coppers, the induced pile-ups are symmetrical along the scratching directions when the scratching directions are parallel to the symmetrical axes of the slip systems. While the pile-ups are asymmetrical for the other two cases, and the pile-up heights located on the left-side of scratching direction are larger than those of the right-side.

Figure 17a–e shows the subsurface deformation of (111)-oriented copper scratched along different directions. The size difference for the main uplifted regions of the selected five cases is relatively smaller. Similarly, a larger region is yielded when the scratched depth is larger.

Conclusions

The deformation behavior of (001)-, (101)- and (111)-oriented coppers under different scratching paths is investigated by CPFEM simulation. The main conclusions can be drawn as follows:

(1) The simulated scratching depth and surface pile-up topography are in good agreement with experimental results. The developed CPFEM model is therefore validated.
(2) Scratching depth is significantly affected by scratching path. The scratching depth changes periodically with respect to the scratching direction, and the periods for (001)-, (101)- and (111)-oriented coppers are 90°, 180° and 120°, respectively.
(3) Various topographies generated in the cases with different scratching paths. The pile-ups are symmetrical when a tip scratches along the

directions paralleled to the symmetrical axes of slip systems.

Acknowledgements

The authors would like to acknowledge the support from National Natural Science Foundation of China (No. 51875373), the Science and Technology Foundation of Sichuan (2019YJ0093) and the Fundamental Research Funds for Central Universities (No. 0060204153006). Q.Z. would also like to acknowledge the supports from the China Postdoctoral Science Foundation (Nos. 2018M643469, 2019T120836).

Declarations

Conflict of interest The authors declare that they have no conflicts of interest.

References

[1] Daiguji H, Yang PD, Szeri AJ, Majumdar A (2004) Electrochemomechanical energy conversion in nanofluidic channels. Nano Lett 4:2315. https://doi.org/10.1021/nl0489945

[2] Malekian M, Park SS, Strathearn D, Mostofa MG, Jun MBG (2010) Atomic force microscope probe-based nanometric scribing. J Micromech Microeng. https://doi.org/10.1088/0960-1317/20/11/115016

[3] Kassavetis S, Mitsakakis K, Logothetidis S (2007) Nanoscale patterning and deformation of soft matter by scanning probe microscopy. Mater Sci Eng C 27:1456. https://doi.org/10.1016/j.msec.2006.08.004

[4] Kawasegi N, Takano N, Oka D et al (2006) Nanomachining of silicon surface using atomic force microscope with diamond tip. J Manuf Sci Eng-Trans ASME 128:723–729

[5] Zambaldi C, Raabe D (2010) Plastic anisotropy of gamma-TiAl revealed by axisymmetric indentation. Acta Mater 58:3516. https://doi.org/10.1016/j.actamat.2010.02.025

[6] Wang Y, Raabe D, Kluber C, Roters F (2004) Orientation dependence of nanoindentation pile-up patterns and of nanoindentation microtextures in copper single crystals. Acta Mater 52:2229. https://doi.org/10.1016/j.actamat.2004.01.016

[7] Liu M, Lu C, Tieu KA, Peng CT, Kong C (2015) A combined experimental-numerical approach for determining mechanical properties of aluminum subjects to nanoindentation. Sci Rep. https://doi.org/10.1038/srep15072

[8] Zhu J, Xiong C, Ma L et al (2020) Coupled effect of scratching direction and speed on nano-scratching behavior of single crystalline copper. Tribol Int. https://doi.org/10.1016/j.triboint.2020.106385

[9] Chavoshi SZ, Xu S (2018) A review on micro- and nano-scratching/tribology at high temperatures: instrumentation and experimentation. J Mater Eng Perform 27:3844. https://doi.org/10.1007/s11665-018-3493-5

[10] Brinckmann S, Dehm G (2015) Nanotribology in austenite: plastic plowing and crack formation. Wear 338:436. https://doi.org/10.1016/j.wear.2015.05.001

[11] Xu N, Han W, Wang Y, Li J, Shan Z (2017) Nanoscratching of copper surface by CeO2. Acta Mater 124:343. https://doi.org/10.1016/j.actamat.2016.11.008

[12] Hodge AM, Nieh TG (2004) Evaluating abrasive wear of amorphous alloys using nanoscratch technique. Intermetallics 12:741. https://doi.org/10.1016/j.intermet.2004.02.014

[13] Vencl A, Manic N, Popovic V, Mrdak M (2010) Possibility of the abrasive wear resistance determination with scratch tester. Tribol Lett 37:591. https://doi.org/10.1007/s11249-009-9556-x

[14] Charitidis CA (2010) Nanomechanical and nanotribological properties of carbon-based thin films: a review. Int J Refract Met Hard Mater 28:51. https://doi.org/10.1016/j.ijrmhm.2009.08.003

[15] Ha S, Jang J-H, Kim K (2017) Finite element implementation of dislocation-density-based crystal plasticity model and its application to pure aluminum crystalline materials. Int J Mech Sci 120:249. https://doi.org/10.1016/j.ijmecsci.2016.11.011

[16] Choi SH, Kim EY, Woo W, Han SH, Kwak JH (2013) The effect of crystallographic orientation on the micromechanical deformation and failure behaviors of DP980 steel during uniaxial tension. Int J Plast 45:85. https://doi.org/10.1016/j.ijplas.2012.11.013

[17] Choi SH, Kim DW, Seong BS, Rollett AD (2011) 3-D simulation of spatial stress distribution in an AZ31 Mg alloy sheet under in-plane compression. Int J Plast 27:1702. https://doi.org/10.1016/j.ijplas.2011.05.014

[18] Wei P, Lu C, Tieu K, Su L, Deng G, Huang W (2017) A study on the texture evolution mechanism of nickel single crystal deformed by high pressure torsion. Mater Sci Eng A 684:239. https://doi.org/10.1016/j.msea.2016.11.098

[19] Wang Z, Zhang J, Xu Z et al (2019) Crystal plasticity finite element modeling and simulation of diamond cutting of polycrystalline copper. J Manuf Process 38:187. https://doi.org/10.1016/j.jmapro.2019.01.007

[20] Wang Z, Zhang H, Li Z et al (2019) Crystal plasticity finite element simulation and experiment investigation of

nanoscratching of single crystalline copper. Wear 430:100. https://doi.org/10.1016/j.wear.2019.04.024

[21] Becker R, Butler JF, Hu H, Lalli LA (1991) Analysis of an aluminum single-crystal with unstable initial orientation (001) 110 in channel die compression. Metall Trans A 22:45. https://doi.org/10.1007/bf03350948

[22] Zhao Z, Ramesh M, Raabe D, Cuitino AM, Radovitzky R (2008) Investigation of three-dimensional aspects of grain-scale plastic surface deformation of an aluminum oligocrystal. Int J Plast 24:2278. https://doi.org/10.1016/j.ijplas.2008.01.002

[23] Zhao Z, Kuchnicki S, Radovitzky R, Cultino A (2007) Influence of in-grain mesh resolution on the prediction of deformation textures in fcc polycrystals by crystal plasticity FEM. Acta Mater 55:2361. https://doi.org/10.1016/j.actamat.2006.11.035

[24] Eisenlohr P, Roters F (2008) Selecting a set of discrete orientations for accurate texture reconstruction. Comput Mater Sci 42:670. https://doi.org/10.1016/j.commatsci.2007.09.015

[25] Raabe D, Roters F (2004) Using texture components in crystal plasticity finite element simulations. Int J Plast 20:339. https://doi.org/10.1016/s0749-6419(03)00092-5

[26] Roters F, Eisenlohr P, Hantcherli L, Tjahjanto DD, Bieler TR, Raabe D (2010) Overview of constitutive laws, kinematics, homogenization and multiscale methods in crystal plasticity finite-element modeling: theory, experiments, applications. Acta Mater 58:1152. https://doi.org/10.1016/j.actamat.2009.10.058

[27] Roters F, Diehl M, Shanthraj P et al (2019) DAMASK–The dusseldorf advanced material simulation kit for modeling multi-physics crystal plasticity, thermal, and damage phenomena from the single crystal up to the component scale. Comput Mater Sci 158:420. https://doi.org/10.1016/j.commatsci.2018.04.030

[28] Wang ZF, Zhang JJ, ul Hassan H et al (2018) Coupled effect of crystallographic orientation and indenter geometry on nanoindentation of single crystalline copper. Int J Mech Sci 148:531–539. https://doi.org/10.1016/j.ijmecsci.2018.09.007